ELSEVIER

Physics of the Earth and Planetary Interiors 93 (1996) 257–268

PHYSICS OF THE EARTH AND PLANETARY INTERIORS

Regional seismic phases across the Ligurian Sea: Lg blockage and oceanic propagation

N. Shapiro [a,*], N. Béthoux [b], M. Campillo [a], A. Paul [a]

[a] *Laboratoire de Géophysique Interne et Tectonophysique, Université Joseph Fourier, BP 53X, 38041 Grenoble Cedex, France*
[b] *Institut de Géodynamique, CNRS, rue Albert Einstein, Sophia Antipolis 1-06560 Valbonne, France*

Received 23 February 1995; revision accepted 1 May 1995

Abstract

The Ligurian Sea (West Mediterranean) is an example of a narrow oceanic basin which stops Lg wave propagation. Locating the exact point of Lg extinction was one of the goals of the SISBALIG II seismological experiment, which deployed both inland stations in Provence and Corsica and Ocean Bottom Seismometers (OBS) in the Ligurian Sea. A precise analysis of all available regional seismological data using energy diagrams reveals the role of the Provence margin in the Lg phase extinction for seismic events occurring in the southwestern Alps. The extinction is not a progressive phenomenon along oceanic travel path but occurs in a narrow zone of about 20 km width in the vicinity of the Provence margin. The extinction is accompanied by the generation of two types of diffracted waves: the mantle phase Sn ($V_s > 3.5$ km s^{-1}), and very low velocity S waves appearing both near the Provence margin and in the middle of the Ligurian basin. We performed numerical simulation of SH wave propagation in two-dimensional (2D) media to investigate the mechanisms of Lg extinction. The simulations confirm that simple crustal thinning at the continent–ocean boundary alone cannot cause the observed extinction of Lg waves, although the change in Moho depth does induce the diffraction of a part of the incident Lg wavetrain into mantle waves, giving rise to the Sn phase on the other side of the basin. The existence of soft oceanic sediments is a very important factor in explaining the extinction, as a large part of the Lg energy is transferred into slow S waves trapped in the sediments. Moreover, comparison of synthetic seismograms and observed data shows that the observed two packets of low-velocity waves are an indication of the asymmetry of the Ligurian basin, with the existence of two shallow basins with very low S velocity (1.0 km s^{-1}) near the Provence margin and in the middle of the Ligurian Sea. However, the attenuation of Lg waves in the vicinity of the Provence margin is more abrupt in the data than in the simulations. This discrepancy could result from the complex geometry of the continent–ocean transition zone and its possibly very diffractive nature, two factors that could add to Lg extinction at the margin and are impossible to take into account in models.

1. Introduction

Observations of the blockage of Lg waves by oceanic crust are numerous. Press and Ewing (1952) first observed a strong attenuation of Lg for propagation paths including an oceanic part of more than 100 km length. The mechanism of this attenuation was investigated by many researchers using a number of theoretical tools (see Cao and Muirhead (1993) for a summary). Most

* Corresponding author.

SSDI 0031-9201(95)03069-7

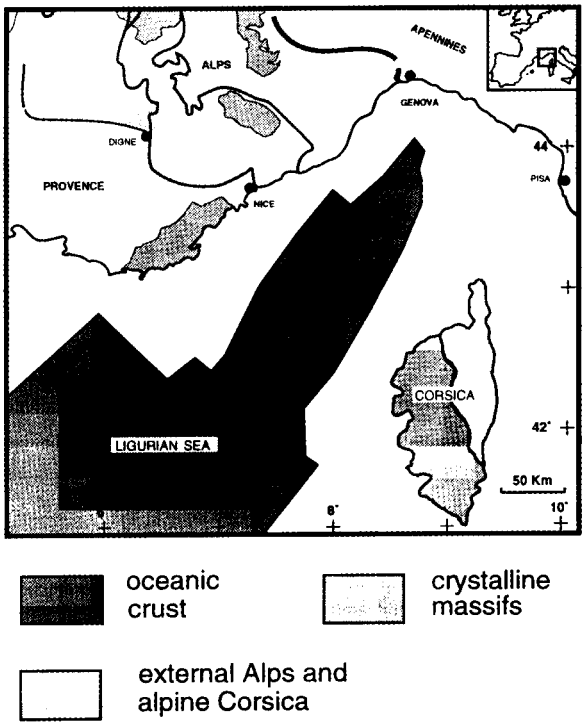

Fig. 1. Tectonic map of the Ligurian Sea. The dark grey central area is oceanic-type basement (according to Réhault (1981)).

of these studies only provide theoretical results without comparison with observed data. To identify the location and understand the mechanism of extinction of Lg waves in an oceanic basin, we set up a temporary network of seismic stations across the Ligurian Sea (Western Mediterranean Sea) from the Provence margin to Corsica during the SISBALIG II experiment (Béthoux et al., 1993).

The Ligurian Sea is a back-arc basin created in the Alpine domain (Fig. 1). Following an Oligocene rifting phase, oceanic accretion occurred between 21 and 18 m.a. B.P. along a spreading axis trending NE–SW (Réhault, 1981). The resulting basin has sharp and narrow margins. It is surrounded by the high topographies of the southwestern Alps and the Apennines. This region is seismically active and a $M_l = 6.0$ event occurred in 1963. The structural framework of the Ligurian Basin is rather well documented by reflection and refraction data (Réhault and Béthoux, 1984; Le Douaran et al., 1984), which indicate that the oceanic crust is restricted to an elongated and narrow zone whose width increases from 50 km in the north to 100 km in the south. However, the exact location of the transition between oceanic crust and stretched continental crust is still debated (Béthoux et al., 1986). In the central part of the basin, the oceanic crust is overlaid by a thick sedimentary sequence including three main layers. A layer of marine Miocene sediments of 2.5–4 km thickness underlies layer of Messinian evaporites of 2 km thickness (including a salt layer thicker than 1 km), and 1 km of pelagic and turbiditic Plio-Quaternary sediments.

It has been observed that Lg waves do not reach the Corsican seismological stations even from events in the southern Alps, in spite of the moderate dimensions of the basin. This is illustrated by the lack of Lg phase picks at the permanent Corsican stations in regional bulletins such as that from LDG (LDG/CEA: Laboratoire de Détection Géophysique du Commissariat à l'Energie Atomique). Consequently, the Ligurian basin is a good laboratory to study propagation of regional phases through a continental margin and an oceanic basin. The small scale of the area of interest made possible the deployment of both inland seismological stations along the northern and the southern coasts and an network of OBS on the continental slopes and in the basin. Data were collected for 3 months in autumn 1992. Owing to limitations in the epicentral distance, the quality of records, and the number of records available, investigations were focused on four regional earthquakes among the 123 events which were recorded. In the first part of this paper, we conduct a thorough analysis of wave amplitudes as a function of station location with respect to the margin, which indicates mechanisms of energy transfers between crustal and mantle phases. In the second part, synthetic seismograms are computed for simple models, to clarify the mechanisms responsible for Lg extinction. Finally, synthetic seismograms for complex models are compared with observations to investigate the influence of the sedimentary cover on Lg wave extinction.

2. Data analysis

The experiment was based on a network of seismic stations of the University of Hamburg and was composed of both OBS and land stations all made from the same electronic components. All stations therefore have the same instrumental response, so there is no need to apply any correction before studying amplitude variations across the array. The sensors were 4.5 Hz three-component geophones. Up to 20 OBS were deployed simultaneously, and the northern and southern inland networks included 42 stations. A total number of 123 events was recorded. Only a small part of this dataset could be used in our study owing to a strong and well-known (Stoll et al., 1991) noise problem at the OBS. Another important constraint in the data selection was the geometry of the network, which changed regularly as a result of movement of the OBS. For the study of Lg wave propagation, we needed records of waves that had travelled along paths almost perpendicular to the basin axis. The third constraint was the epicentral distance, which had to be large enough to observe Lg waves. We finally selected four events located in the southern Alps, as listed in Table 1. The first two were recorded by inland stations in southern France and Corsica

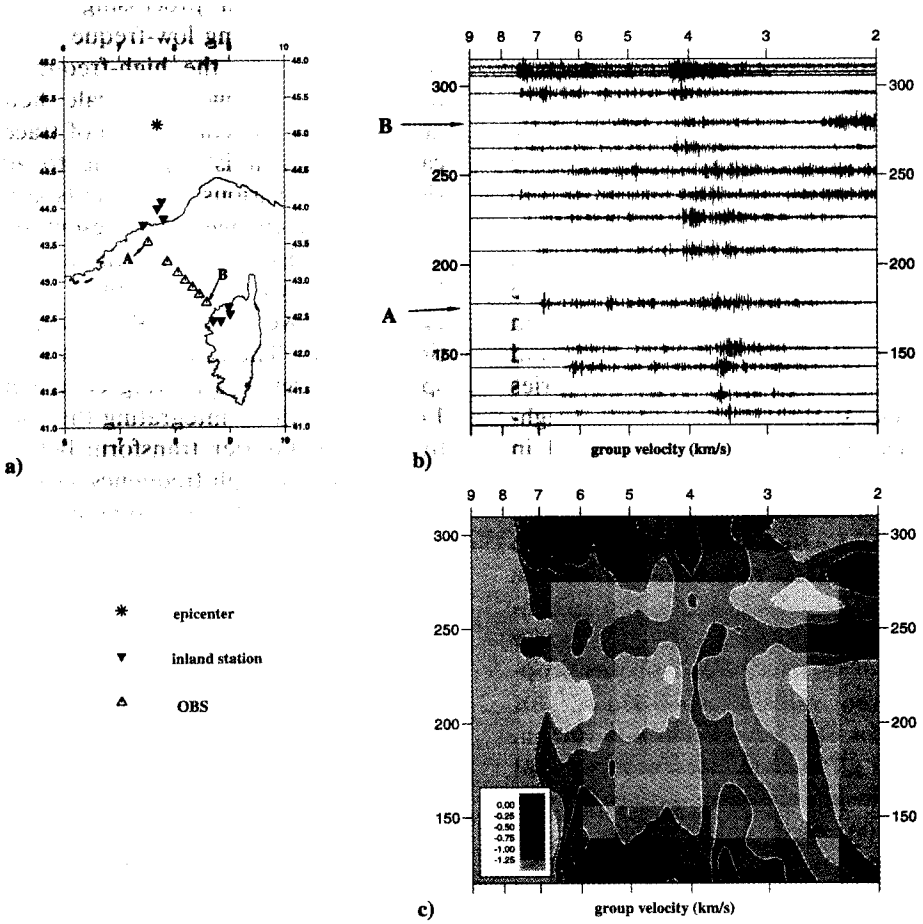

Fig. 2. Dataset for Event 1 (Table 1). (a) Location map of epicentre and stations. (b) Normalized vertical component seismograms plotted as a function of epicentral distance and group velocity (A and B show the first and last OBS of the profile). (c) Energy diagram calculated from seismograms plotted in (b) (see text for further explanations). Values of energy have been normalized to make the absolute maximum equal to unity, and transformed using decimal logarithms.

Table 1
Parameters of earthquakes used in this study (locations were computed using both permanent and temporary stations)

N	Day	Month	Year	Hour	Min	Lat.	Long.	Depth	M_l
1	13	09	1992	5	0	45.13	7.68	9	3.6
2	14	09	1992	13	20	45.02	6.76	1	3.0
3	27	10	1992	03	12	44.49	7.26	1	3.0
4	11	11	1992	00	59	44.48	7.24	4	3.1

and by OBS installed along a profile across the Ligurian Sea. Events 3 and 4 were recorded by OBS located in the vicinity of the Provence margin. We used 15 sets of three-component records for Event 1, and 12, four and two records for Events 2, 3 and 4, respectively. The locations of epicentre and stations are shown in Fig. 2(a).

The data analysis starts by considering the vertical-component records of Event 1 (Fig. 2). The first processing step was restricted to the vertical components because it was impossible to separate transverse and radial motion as the azimuthal orientation of the sensors was not known. Seismograms with amplitudes normalized to the absolute maximum of each trace are plotted in Fig. 2(b). The normalization is introduced to avoid the effect of local amplification, which varies strongly from one station to another for high-frequency signals. The main trend observed in the row amplitudes is a strong attenuation across the basin: maximum amplitudes are, on average, ten times weaker in Corsica than in Provence. In Fig. 2(b) the travel time t is replaced by the group velocity u ($u = d/t$, where d is the epicentral distance) on the horizontal axis to simplify the identification of various seismic phases propagating with different velocities (6–8 km s^{-1} for Pn, 5–6 km s^{-1} for Pg, 3.7–4.5 km s^{-1} for Sn, 3–3.5 km s^{-1} for Lg). Fig. 2(b) clearly shows that the most energetic phase is Lg (group velocity 3–3.3 km s^{-1}) on seismograms recorded in Provence (distance range 110–150 km). At Corsican stations (290–310 km), the large-amplitude S wave has a group velocity of about 4 km s^{-1}. This is too fast for a crustal wave and it must be interpreted as the mantle phase Sn with some possible delay. This first observation characterizes the main phenomenon we want to study, i.e. the blockage of Lg waves by oceanic crust.

Our purpose is to study the progressive changes in the S wavefield across the basin associated with diffractions and energy exchanges between seismic phases as a result of to the lateral variations of the crustal structure. The limited number of data available make it necessary to find the representation which uses simultaneously all the available information to obtain the most accurate image of the process. This representation must include signals corresponding to different events as well as differently oriented components of motion beacause of the problem of sensor orientation. The direct use of raw time series is not convenient for our processing for two reasons. First, the interesting low-frequency energy variation is hidden by the high-frequency variations induced by shallow small-scale heterogeneities and therefore the comparison of traces is complicated; second, it is impossible to add the time signals of the various components at each station. Therefore we change the representation and build spectral energy maps using the following process. First, we apply a band-pass filter in the range 3–7 Hz to improve the signal-to-noise ratio in the time domain. The second step is to compute the spectral energy in a moving Gaussian window of 1.4 s halfwidth by integrating the squared amplitude of the Fourier transform between 3 and 7 Hz. The initial high-frequency seismogram is replaced by this positive function, which varies slowly with time (or group velocity). The comparison between signals is thus simplified; furthermore, this representation make it possible to add the contribution of all components at each station. The third step is a normalization of energy curves with respect to the energy of the Sn phase, or, more exactly, to the maximum of energy in the group velocity window 3.7–3.95 km s^{-1}. This is used to evaluate the energy ratio between crustal and mantle S waves. As Sn and Lg waves can be assumed to be affected in the same way by local site amplification effects, the normalization also makes it possible to remove much of the local amplitude effects which are outside the scope of this study. After these three processing steps, we obtain a map of energy variations with group

velocity and space which is irregularly sampled in space. The fourth step is to interpolate data to the whole range of epicentral distances using a bilinear interpolation to draw a contour map in the epicentral distance–group velocity plane. Fig. 2(c) shows such a map of the energy distribution calculated using the vertical-component seismograms of Fig. 2(b). The map shows that Lg remains the largest energy phase until the epicentral distance of 160–170 km. At larger distances, the energy maximum moves to faster S group velocities ($V_s > 3.5$ km s^{-1}). A comparison with seismograms of Fig. 2(b) shows that this change in the type of S-wave propagation is located between the last inland station and the first OBS (A in Fig. 2(a)) in the vicinity of the Provence margin. This fast phase remains dominant across the profile and S waves reach Corsica with a velocity of about 4 km s^{-1}. Another remarkable phenomenon is the generation of very slow waves in the central and southern parts of the basin. The behaviour of P waves is similar. The Pg phase is dominant until the Provence margin, where a faster phase appears and becomes dominant in Corsica.

Fig. 3 presents the result of the four-step analysis applied to vertical-component records of Event 2. Despite the smaller number of stations available and the significant difference in epicentre location, the main features of the energy distribution are similar for both events. Fig. 3 shows the extinction of Lg waves in the vicinity of

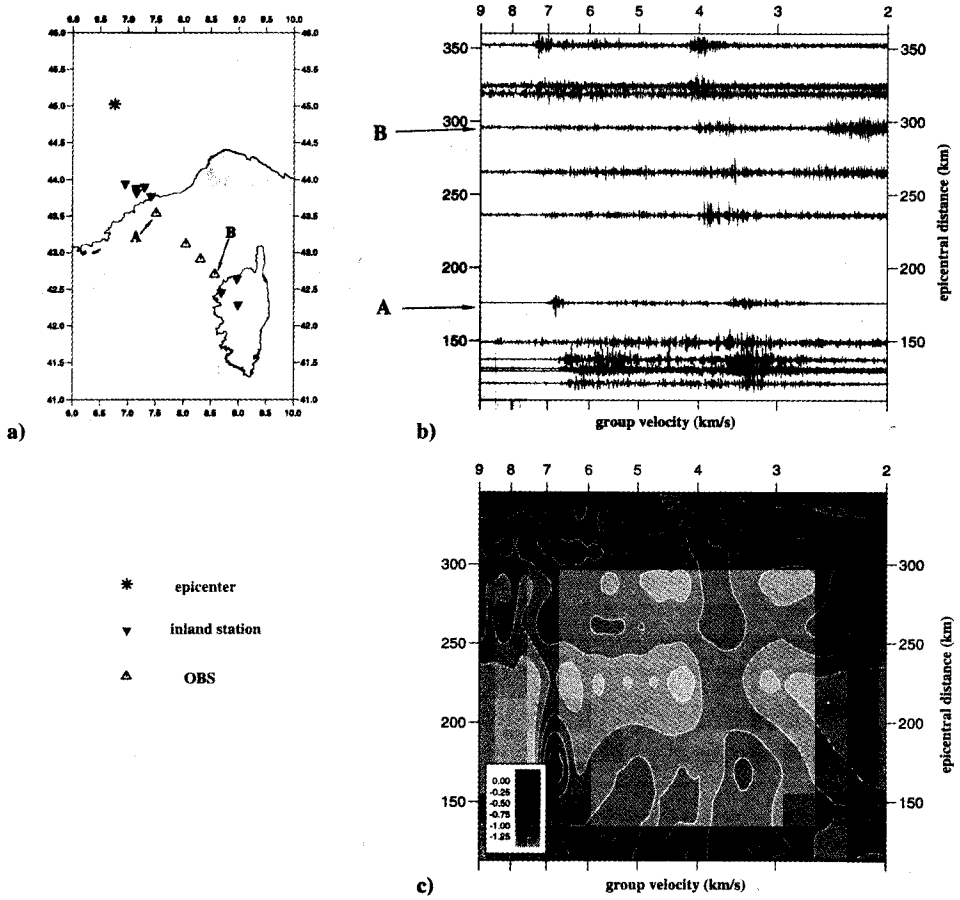

Fig. 3. Dataset for Event 2 (Table 1). Same legend as for Fig. 2.

the northern margin, the mantle S-wave arrival in Corsica ($V_s = 4$ km s^{-1}) and the generation of an energetic packet of very low velocity waves in the middle of the basin.

For both events the number of stations available in the vicinity of the northern margin is small and it is difficult to identify the exact location of Lg extinction using individual energy diagrams. To enhance the spatial coverage near the margin we build a composite energy map using all the three-component records for all four events (Fig. 4(a)). Normalized spectral energies are computed first from each seismogram through the three-step process described above. Then, energies of all components are added for each station. The next step is to use a distance scale which is independent of the event location. As shown in Fig. 4(a), the epicentral distance is replaced in the composite map by the distance *dm* between the station and the foot of the Provence margin. This location is used as the reference point because it seems to be the place where Lg disappears, as shown previously with records of Events 1 and 2. Considering that all events are located north of the margin, the distance *dm* is taken as negative for stations located north of the margin, and positive for stations located south of it. The last step is bilinear interpolation. Fig. 4(b) shows the resulting energy distribution. The horizontal dotted lines correspond to the locations of the stations. They show how this processing improves the spatial sampling rate. The main features of this energy distribution confirm and locate more precisely in space the observations from Events 1

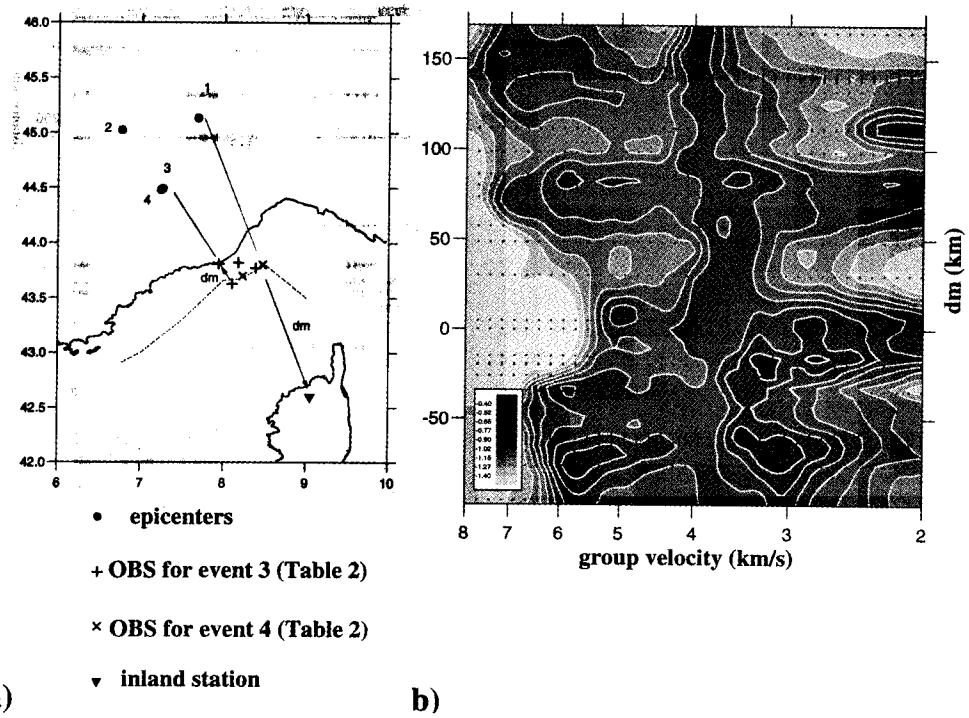

Fig. 4. Composite energy map built from all the available components of the four regional events used in the study. (a) Location map showing the four epicentres and OBS locations for Events 3 and 4. The dashed line gives the location of the foot of the Provence margin and the continuous lines show how the epicentral distances are converted into distances to the margin (*dm*) used as the coordinate along the vertical axis of (b). (b) Final composite energy diagram. The dotted lines show the locations of observations.

and 2. Moreover, the records of OBS near the margin reveal the existence of another packet of slow waves in this area.

To summarize, Fig. 4(b) shows that: (1) the Lg wave extinction is not a widespread phenomenon but occurs in a narrow zone of about 20 km width in the vicinity of the Provence margin; (2) the extinction appears to be accompanied by the generation of two types of diffracted waves: the mantle phase Sn ($V_s > 3.5$ km s^{-1}), and very low velocity waves appearing near the Provence margin and in the middle of the Ligurian basin. These observations make us consider several hypotheses for the mechanism of Lg extinction. As we have seen that Lg disappears in the vicinity of the margin, we can suppose extinction to be due to the structure of the continent–ocean transition zone. More precisely, it could originate either in the geometry of the Moho beneath the margin or in the change in the crustal structure. Moreover, the observation of slow waves which probably propagate in soft oceanic sediments indicates that the shallow sedimentary layers could play an important part in Lg extinction. These hypotheses will be investigated below using numerical simulation of wave propagation in heterogeneous media.

3. Numerical simulations

The phenomenon of Lg wave blockage by an oceanic travel path has been investigated theoretically by several researchers. Using two-dimensional (2D) ray diagrams in a single layer over a half-space, Kennett (1986) suggested that the diffraction caused by the change in Moho dip at the margin can result in a significant attenuation of the waves trapped in the crust. Campillo (1987) and Campillo et al. (1993) computed SH synthetic seismograms in multilayered models with variations in Moho depth. They showed that a thinning of the crust induces a significant attenuation. However, it is not sufficient to extinguish completely Lg waves. Using a combination of the propagator matrix and finite element methods, Regan and Harkrider (1989) came to the same conclusion. So did Maupin (1989), who used the coupled local modes method to study the propagation of Lg waves across the slightly more complicated 2D structures of the North Sea. Cao and Muirhead (1993) modelled Lg wave propagation in the 2D P–SV case using finite difference techniques. They concluded that the water layer plays an important part in the Lg wave extinction owing to the coupling of P–SV elastic waves with acoustic waves in the water. However, this conclusion is not valid for the SH component which makes up a large part of Lg.

Here we use the boundary integral equation method (BIEM) coupled with the discrete wavenumber technique to calculate SH seismograms in a 2D heterogeneous medium (Bouchon et al., 1989). The 2D approximation is justified in our case because the Ligurian basin has approximately a 2D structure and the waves propagate almost perpendicular to it for all the data we intend to compare with synthetics. The Lg arrival can be considered as the superposition of post-critically reflected S waves in the crust (see Campillo (1990) for a review of interpretation of Lg). The behaviour of Lg is therefore similar for both its SH and P–SV components, so the consideration of the SH component only is sufficient to simulate the main properties of the complete phase. A 2s Ricker wavelet was used as the source time function. Owing to limitations in computer memory, the maximum frequency computed in synthetics is lower than 1 Hz in all the models. This is much less than the dominant frequency of observed data. However, Gibson and Campillo (1994) showed, by comparing BIEM solutions with high-frequency dynamic ray tracing solutions, that for relatively simple structures such as those we are going to study here, the results of low-frequency and high-frequency simulations have similar characteristics. This result implies that the low-frequency simulations can be used to interpret high-frequency observations.

We first investigate a set of simple models to study the effect on Lg propagation of individual features such as Moho uplift or presence of sedimentary layers. The reference model is a simple flat-layered model with the continental crust (Layer 5 in Table 2, $V_s = 3.65$ km s^{-1}) overlying the mantle (Layer 7 in Table 2, $V_s = 4.7$ km s^{-1}).

Table 2
Elastic parameters of the various layers used in the models

N	V_s	Density	Q_s	Description
1	1.0	2.1	20	Shallow sediments (type 2)
2	1.3	2.1	20	Shallow sediments
3	2.7	2.6	50	Oceanic sediments
4	3.65	2.9	20	Continental crust (low Q)
5	3.65	2.9	400	Continental crust (high Q)
6	4.2	3.0	400	Oceanic crust
7	4.7	3.3	1000	Mantle

The source–receiver configuration is the same in all simulations. The source is buried at 15 km depth and 26 receivers are located on the surface every 10 km between 100 and 350 km epicentral distance. The model and resulting synthetic seismograms are shown in Fig. 5(a). As expected, the main wavetrain is Lg, which propagates in the crustal waveguide with a group velocity between 3.4 and 3.6 km s^{-1}.

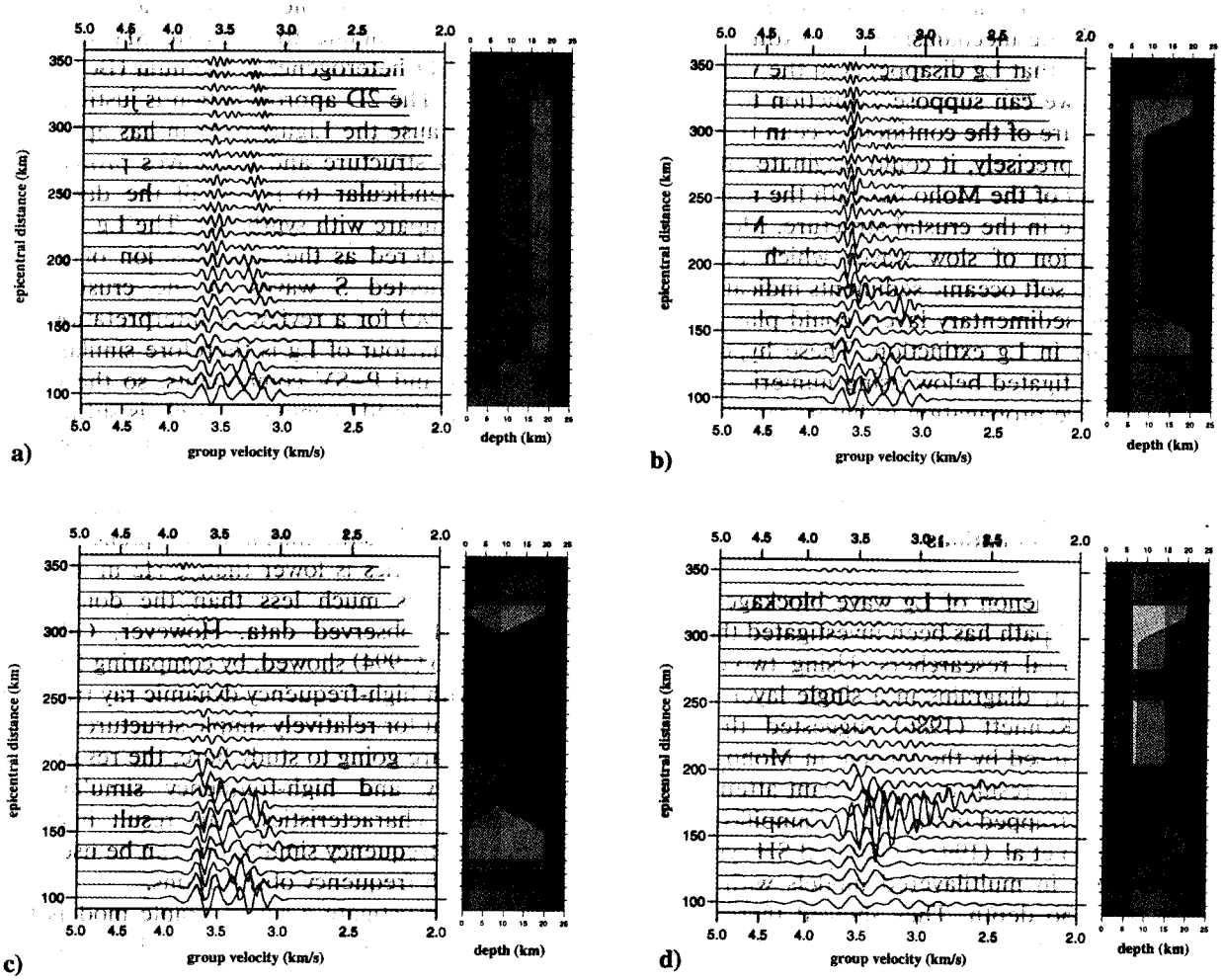

Fig. 5. Synthetic seismograms computed for the first four models. The crustal cross-sections are plotted in the left-hand side of each section at the same vertical scale; the depth scale is exaggerated by a factor of three. All seismograms are plotted at the same amplitude scale to facilitate comparison. The maximum frequency computed for models shown in (a), (b) and (c) is 1 Hz, and is 0.7 Hz for model shown in (d). (a) Reference model. (b) Model with crustal thinning. (c) Same model as in (b), except that the thinned crust of the basin has $Q = 20$. (d) Same as (b) with a low-velocity shallow layer.

We first perturb the reference model by introducing a change in crustal thickness beneath the margin, with a geometry similar to that assumed for the region under study (Fig. 5(b)). According to seismic data (Réhault, 1981), the Moho depth decreases from 20 km beneath the Provence coast to 8 km at a distance of 25 km offshore. The layer velocities are the same as in the reference model and the Moho topography is approximated by a cosine function. The main result shown by Fig. 5(b) is that the change in crustal thickness does not inhibit Lg wave propagation through the basin. After the second margin (i.e. at source–receiver offsets greater than 320 km) the main arrival still has a group velocity of 3.5–3.6 km s^{-1}, which corresponds to crustal propagation as Lg. However, a slight attenuation of the Lg phase is observed and faster waves appear at large distances on the other side of the basin. Another difference from the reference model is a slight perturbation of waveforms in the vicinity of the first margin (distances 160–190 km), probably as a result of focusing and de-focusing phenomena at the Moho topography. Therefore, we conclude that the change in thickness of the crustal waveguide locally perturbs the waveforms and induces a slight attenuation of Lg because a part of the incident wavefield is diffracted into the mantle. However, the observed total extinction of Lg waves cannot be explained by the crustal thinning only.

To illustrate the diffraction of Lg into mantle waves at the margin, a strong attenuation ($Q = 20$) is introduced in the thinned crust to stop Lg propagation (Fig. 5(c)). As a logical result, all the waves trapped in the crust are strongly attenuated, making it possible to observe S waves reaching the last stations with a group velocity of 3.7–3.9 km s^{-1}. The high velocity indicates that these S waves are Sn. They propagate as Lg before reaching the first margin, where they are diffracted into the mantle. A part of the diffracted wavetrain then propagates as Sn beneath the basin and is recorded at the distant stations with high group velocities.

An important characteristic of the oceanic crust is the presence of shallow soft sediments. The importance of these low-velocity layers for the scattering of Lg wave energy was shown by Knopoff et al. (1979) by analysis of dispersion properties of the higher modes of surface waves. In the case of the oceanic crust, the contribution of the various higher modes does not give rise to a clear wave packet in a narrow group velocity window as is the case for the continental crust. In oceanic crust, most of the energy at high frequencies remains trapped in the shallow low-velocity layers. However, the low Q factor and strong

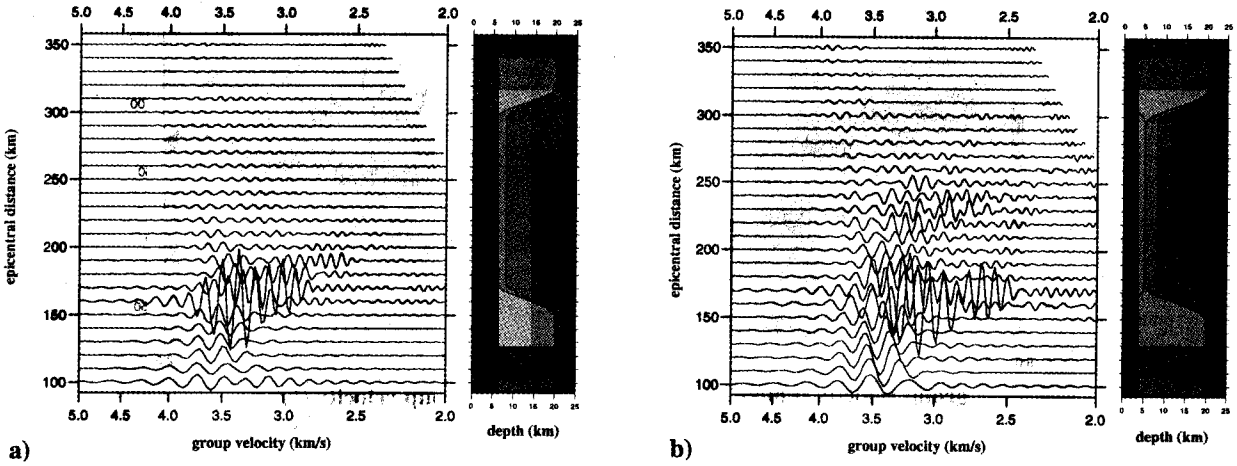

Fig. 6. Synthetic seismograms computed for the two final models. (a) Model with the three-layered structure of the oceanic basin deduced from refraction and reflection data. (b) Same model with the shallow low-velocity layer of (a) divided into two separate basins.

heterogeneity of the sediments induce a rapid destruction of the trapped waves. To investigate the effect of the sediments, we add a slow shallow layer with a strong attenuation (Layer 2 in Table 2: $V_s = 1.3$ km s^{-1}, $Q_s = 20$) to the model with crustal thinning (Fig. 5(d)). Synthetic seismograms clearly show the generation of low group velocity waves ($V_s < 2.5$ km s^{-1}) near the first margin, which induces a strong local amplification at 160 km offset. Within the basin itself (160–320 km), the crustal guided waves are strongly dispersed, so the duration of the wavetrain is significantly increased. After crossing the second margin, the wavetrain is dominated by high-velocity mantle waves.

The last step is to study more realistic models based on seismic refraction and reflection data (Réhault, 1981; Le Douaran et al., 1984). The three layers of the oceanic basin are taken into account: shallow soft sediments (Layer 2 in Table 2: $V_s = 1.3$ km s^{-1}), consolidated sediments (Layer 3 in Table 2: $V_s = 2.7$ km s^{-1}) and a high-velocity basement (Layer 6: $V_s = 4.2$ km s^{-1}). The resulting seismograms (Fig. 6(a)) do not differ strongly from those of the previous model (Fig. 5(d)). We still observe a local amplification near the first margin induced by slow waves propagating in the shallow sediments, and a fast S-wave arrival ($V =$ 3.7–3.9 km s^{-1}) after the second margin which is the diffracted Sn phase. The similarity of the seismograms for these two models (Figs. 5(d) and 6(a)) proves that the most prominent effect is that of the shallow low-velocity layer, and that the deeper and faster layers are of much less importance to Lg diffraction. With this simple but realistic structure of the oceanic crust, we succeed in simulating the Lg blockage at the first margin and the generation of very slow waves in oceanic sediments — both phenomena observed in the real data. The main difference remaining between the observations and the synthetics is the existence of two packets of slow waves in the data — one after the first margin and the other in the middle of the basin (Fig. 4). In fact, gravity data (Klingelé et al., 1991) and heat flow data (Jemsek et al., 1985; Burrus and Foucher, 1986), indicate that the structure of the northern and southern parts of Ligurian basin are different. This asymmetry is interpreted as the result of an abnormally rapid tectonic subsidence of the Alpine–Provençal margin, as indicated by the large sediment thickness for this recent basin. Moreover, the spreading rate is larger towards the Corsica–Sardinia block than towards the northwest (Pasquale et al., 1994).

Accounting for the asymmetry of the basin, the

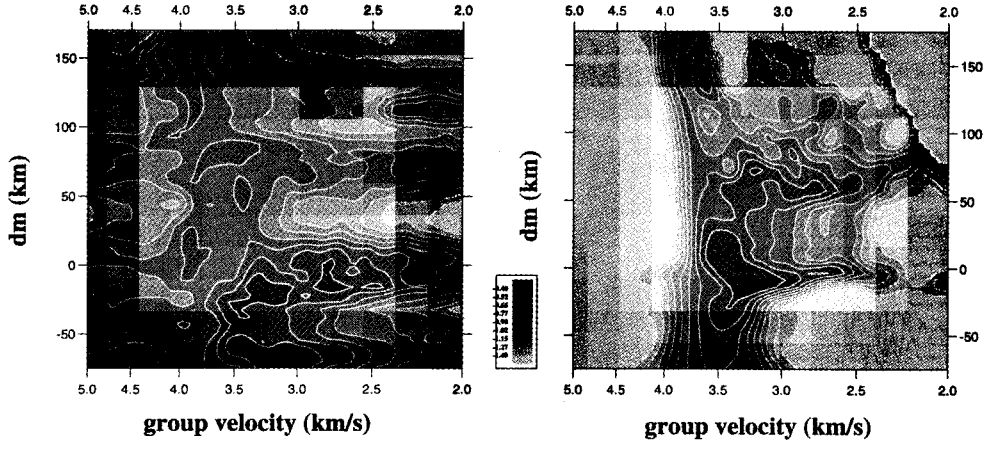

Fig. 7. Final comparison between observed and simulated energy diagrams. In both plots, the distance to the margin *dm* is used as the coordinate along the vertical axis. (a) Observations (same plot as Fig. 4). (b) Synthetic data computed for the best-fitting model of Fig. 6(b).

single low-velocity shallow layer in Fig. 6(a) is replaced by two distinct sedimentary basins, as shown in Fig. 6(b). The northern basin could be associated with the foot of the Provencal margin and the southern one with the zone of high spreading rate. The velocities in the sediments are slightly lowered to account for the abrupt appearance of the slow wave packets in the data (Layer 1 in Table 1: $V_s = 1.0$ km s^{-1}). As a result, two packets of slow waves are generated at 160 and 220 km. The waveform is modified at the last stations with a decrease of the duration of the S-wave arrival owing to a stronger attenuation of waves with group velocities between 3.7 and 3.8 km s^{-1}.

The results of the comparison between the observations and the best-fitting model are summarized in Fig. 7, where the composite energy map of Fig. 4(b) is compared with the energy diagram computed from the synthetics of Fig. 6(b). As pointed out above, the use of smoothed energy diagrams makes the comparison easier, as the processing emphasizes the main low-frequency amplitude variations with epicentral distance and group velocity. The energy diagram for the synthetics is obtained as explained above for the data, but because of the difference in spectral bandwidth, the corners of the band-pass filter and the width of the time window have been changed to 0–0.7 Hz and 2.8 s, respectively. The reference point for distance measurements is taken at the wedge of the crustal thinning located 175 km from the source in Fig. 6(b). As for the data, energies are normalized with respect to their maxima in the group velocity window 3.7–3.95 km s^{-1}. Fig. 7 brings out a number of similarities between simulated and observed data. The group velocity of the S-wave arrival after crossing the basin is about 4 km s^{-1} both in the data and the synthetics. We have seen that it can be interpreted as the Sn phase resulting from the diffraction of a part of the incident Lg into mantle waves at the first margin. Two packets of very slow waves owing to the trapped energy in the soft and shallow sediments are also clear in both diagrams. The most important difference between Fig. 7(a) and Fig. 7(b) is the energy pattern in the vicinity of the first margin. The extinction of the Lg phase appears to be more abrupt in the data than in the model. This difference could be due to the lower spatial resolution of observations in the region of the margin, or to a parasitic effect of normalization which can be influenced by the presence of strong P-wave coda in the data. However, we think that this discrepancy could also indicate that the structure of the continent–ocean boundary is different from the very simple and abrupt transition we assumed in the models. For example, a thicker transition zone with progressive alteration of the continental crust could act as a very efficient barrier for Lg propagation.

4. Conclusions

The set of seismological data collected during the SISBALIG II experiment using both inland networks in Provence and Corsica and OBS in the Ligurian Sea made it possible to conduct a precise study of the progressive changes in the characteristics of the regional waveforms across the oceanic Ligurian basin and its margins. The grouping together of all available regional seismograms in a composite energy diagram demonstrates the part played by the Provence margin in the Lg phase extinction. It appears that the Lg wave extinction is not a widespread phenomenon but occurs in a narrow zone of about 20 km width in the vicinity of the Provence margin. The extinction is accompanied by the generation of two types of diffracted waves: the mantle phase Sn ($V_s > 3.5$ km s^{-1}), and very low velocity S waves that appear both near the Provence margin and in the middle of the Ligurian basin.

The results of numerical modelling confirm that simple crustal thinning at the continent–ocean boundary cannot alone cause the observed extinction of Lg, although the change in Moho depth does induce the diffraction of a part of the incident Lg wavetrain into mantle waves, giving rise to Sn on the other side of the basin. The results also show that the existence of oceanic soft sediments is a very important factor in explaining the extinction, as a large part of the Lg energy is transferred into slow S waves trapped in

the sediments. The computed waveforms strongly depend upon the geometry and wave velocity of the shallow layer with the lowest velocity. The influence of the deeper oceanic structure is much less important and is hidden by the effect of the soft sediments. Moreover, comparison of synthetics and data shows that the observed two packets of low-velocity waves is an indication of the asymmetry of the Ligurian basin, with the existence of two different shallow basins with very low S velocity (1.0 km s^{-1}) near the Provence margin and in the middle of the Ligurian Sea. However, the attenuation of Lg waves in the vicinity of the Provence margin is more abrupt in the data than it is in the simulations. This discrepancy could result from the difficulty in taking into account in the models a complicated geometry of the continent–ocean transition zone and the possibly very diffractive nature of this zone, which are factors that could add to Lg extinction at the margin.

Acknowledgements

We are very grateful to the SISBALIG II team, which included members from the Universities of Hamburg, Genoa, Paris, Nice and Grenoble. Our special thanks are due to Jacques Deverchère and Knuth Lange, who installed and picked up the OBS network whatever the weather conditions. We also thank Christine Fontaine for digitizing and preprocessing the data, Jean-Pierre Réhault for fruitful discussions, and Helle Pedersen for a critical review of the manuscript. This work was supported by INSU–CNRS through project 'A.A. Tomographie'. Numerical computations were performed at the Centre de Calcul Intensif de l'Observatoire de Grenoble.

References

Béthoux, N., Petit, F., Réhault, J.P., Massinon, B. and Montagner, J.P., 1986. Several location methods for underwater shots in the gulf of Genoa (Western Mediterranean): structural implications. Tectonophysics, 128: 357–379.

Béthoux, N., Deverchère, J., Lang, K., Cattaneo, M., Fontaine, C., Campillo, M., Deschamps, A., Eva, C., Ferrandini, J., Gaffet, S., Gauthier, J., Makris, J., Paul, A. and Virieux, J., 1993. Sisbalig II: a sea–land experiment in Occidental Mediterranean Sea. EOS Trans. Am. Geophys. Union, 74: 444.

Bouchon, M., Campillo, M. and Gaffet, S., 1989. A boundary integral equation–discrete wavenumber representation method to study wave propagation in multilayered media having irregular interfaces. Geophysics, 54: 1134–1140.

Burrus, J. and Foucher, J.P., 1986. Contribution to the thermal regime of the Provençal basin based on flumed heat flow surveys and previous investigations. Tectonophysics, 128: 303–334.

Campillo, M., 1987. Lg wave propagation in a laterally varying crust and the distribution of the apparent quality factor in central France. J. Geophys. Res., 92: 12604–12614.

Campillo, M., 1990. Propagation and attenuation characteristics of the crustal phase Lg. Pure Appl. Geophys., 132: 1–19.

Campillo, M., Feignier, B., Bouchon, M. and Béthoux, N., 1993. Attenuation of crustal waves across the Alpine range. J. Geophys. Res., 98: 1987–1996.

Cao, S. and Muirhead, K.J., 1993. Finite difference modelling of Lg blockage. Geophys. J. Int., 115: 85–96.

Gibson, R.L. and Campillo, M., 1994. Numerical simulation of high- and low-frequency Lg wave propagation. Geophys. J. Int., 118: 47–56.

Jemsek, J., Von Herzen, R., Réhault, J.P., Williams, D.L. and Sclater, J.G., 1985. Heat flow and lithospheric thinning in the Ligurian basin (N.W. Mediterranean). Geophys. Res. Lett., 12: 693–696.

Kennett, B.L.N., 1986. Lg waves and structural boundaries. Bull. Seismol. Soc. Am., 76: 1133–1141.

Klingelé, E., Lahmeyer, B. and Freeman, R., 1991. The EGT Bouguer gravity compilation. Tectonophysics, 195: 437–441.

Knopoff, L., Mitchel, R.G., Kausel, E.G. and Schwab, F., 1979. A search for the oceanic Lg phase. Geophys. J.R. Astron. Soc., 56: 211–218.

Le Douaran, S., Burrus, J. and Avedik, F., 1984. Deep structure of the northwestern Mediterranean: a two-ship seismic survey. Mar. Geol., 55: 325–345.

Maupin, V., 1989. Numerical modelling of Lg wave propagation across the North Sea. Geophys. J. Int., 99: 273–283.

Pasquale, V., Verdoya, M. and Chiozzi, P., 1994. Types of crust beneath the Ligurian Sea. Terra Nova, 6: 255–266.

Press, F. and Ewing, M., 1952. Two slow surface waves across North America. Bull. Seismol. Soc. Am., 42: 219–228.

Regan, J. and Harkrider, D.G., 1989. Numerical modelling of SH Lg waves in and near continental margins. Geophys. J. Int., 98: 107–130.

Réhault, J.P., 1981. Evolution tectonique et sédimentaire du Bassin Ligure (Méditerranée Occidentale). Thèse d'Etat, Université Paris.

Réhault, J.P. and Béthoux, N., 1984. Earthquake relocation in the Ligurian Sea (Western Mediterranean): geological interpretation. Mar. Geol., 55: 429–445.

Stoll, R.D., Bryan, G.M. and R. Mithal, 1991. Field experiments to study seafloor seismoacoustic response. J. Acoust. Soc. Am., 89: 2232–2245.